ISBN: 978-3-95450-233-2 ISSN: 2673-5504 doi:10.18429/JACoW-SRF2021-THPFDV002

THE INFLUENCE OF THE IRRADIATION ON THE CURRENT CARRYING PHENOMENA IN HTc MULTILAYERED SUPERCONDUCTORS

J. Sosnowski*, NCBJ, Swierk, Poland

Abstract

In the paper is theoretically investigated the influence of the irradiation arising during the work of SRF accelerators, on the current carrying phenomena appearing at HTc multilayered superconductors. The impact of the concentration and size of created then nano-defects, acting as pinning centers capturing the vortices is considered. The influence of the physical parameters such as magnetic field and temperature on the critical current is regarded too. The critical current analysis is applied then to investigations of the losses generated in the superconducting current leads to the accelerator's electromagnets.

INTRODUCTION

Proper work of the modern accelerators containing the superconducting elements as windings of coils or cover of the resonating cavities, as well as current leads to electromagnets is dependent on the superconducting materials parameters, especially their critical current [1]. These materials, such as multilayered HTc superconductors are however very delicate structures sensitive to mechanical defects introduced for instance by the bending strain [2] during the coil winding procedure. Defects are created too during the work of RF accelerators, as built in Poland PolFEL, which generate then irradiation, including fast neutrons arising as the result of fall RF-waves on the accelerator walls. To the analysis of the influence nano-defects on the current carrying phenomena is devoted just present paper. Research will be performed basing on elaborated model of the interaction pancake vortices specific for multilayered superconductors with pinning centers created just during irradiation process. The results of critical current analysis will be useful for determining then the electromagnetic losses generated in the superconducting current leads to electromagnets. Therefore considered here issue of the influence of irradiation on the properties of these fragile HTc superconducting materials is very important from pure scientific as well as technical point of view.

INFLUENCE OF IRRADIATION ON JC

The influence of the nano-sized defects created especially by the RF irradiation and in secondary way through fast neutrons striking the HTc superconductors was analysed basing on the general equation [2, 3]:

$$F(r_1,..,r_N) = \sum_{i=1}^{N} U(r_i) + \frac{1}{2}\sum_{i\neq j}^{N} F_{inter}(r_i - r_j) - J\emptyset_0 \sum_{i=1}^{N}(l_i - r_i) - \sum_{i=1}^{N} \frac{C(r_i-\xi)^2}{2} V_i \quad (1)$$

Equation (1) describes the energy of N magnetic pancake vortices, specific for layered superconductors, captured on the pinning centers at positions $r_1,..r_N$. U is pinning potential of the captured pancake vortices, while summation runs over N captured magnetic vortices, each of them is transporting quantized magnetic flux $\Phi_0 = 2.07 \cdot 10^{-15}$ Wb. Second expression in Eq. (1) describes the contribution to system energy connected with inter-vortex interaction, while third term is connected with Lorentz force. J is here electric current density, while last part in Eq. (1) describes the increase of the elasticity energy of the vortex lattice during the shift of the vortex from equilibrium position at the process of the magnetic flux capturing. V_i describes connected with this deformation volume, while C is spring constant of the vortices lattice. The geometry of the full capturing of the pancake vortex of the cross-section core area S, on cuboid pinning center of the width d is shown in Fig. 1. In the present paper it has been considered the individual vortex – pinning center interaction, it is neglecting the inter-vortex interaction term. Shift of this vortex from the equilibrium initial position shown in Fig. 1, is connected with Lorentz force induced by current flow, tearing off the vortices and leads to the enhancement of system energy. As the result of this movement the potential barrier arises, which maximal value ΔU appears for the shift of vortex onto distance x_m and is described then by the relation:

$$\Delta U(x_m) = \frac{\mu_0 H_c^2}{2} l\xi^2 \left(arcsin\frac{x_m}{\xi} - \frac{\pi}{2} + arcsin\left(\frac{d}{2\xi}\right) + \frac{x_m}{\xi}\sqrt{1-\left(\frac{x_m}{\xi}\right)^2} + \frac{d}{2\xi}\sqrt{1-\left(\frac{d}{2\xi}\right)^2} \right) - JB\pi\xi^2 l x_m \quad (2)$$

In Eq. (2) valid for the case of the half captured initially pancake type vortices H_c is thermodynamic critical magnetic field, μ_0 magnetic permeability of the vacuum, while l the thickness of the superconducting layer. x_m as it was mentioned before is value of the shift of the vortex against equilibrium position inside the defect onto the distance for which potential barrier reaches the maximum. It arises therefore the energy barrier, which should cross vortex during the flux creep process. In Fig. 1 is shown the geometry of the cross-section of the fully captured vortex inside the nano-sized defect. The radius of the vortex core shown in Fig. 1 is equal to the coherence length ξ. Enhancement of the current in static magnetic field B leads to the increase of the Lorentz force term in Eq. (1), tearing off the vortices from the initial equilibrium position and decreases in this way the potential barrier ΔU. This effect is well seen, if to

*sosnowski.jacek@wp.pl

ISBN: 978-3-95450-233-2 ISSN: 2673-5504 doi:10.18429/JACoW-SRF2021-THPFDV002

pass then from the Cartesian coordinates system to the current representation, which directly indicates that potential barrier decreases continously at the increasing current.

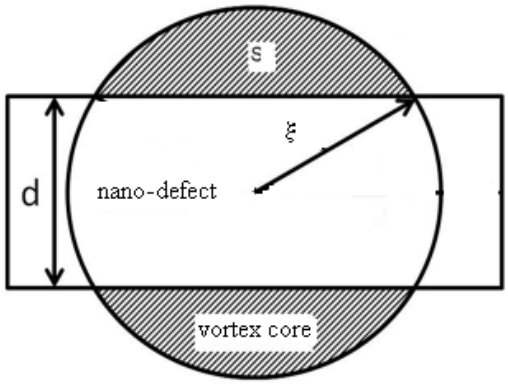

Figure 1: Configuration of the fully captured pancake vortex core of the size ξ and core area S inside the pinning centre of the width d< 2 ξ.

Finally potential barrier vanishes for the current equal to the critical, as it shows Eq. (3):

$$\Delta U(i) = \frac{\mu_0 l \xi^2 H_c^2}{2}\left(\begin{array}{c} arcsin\left(\frac{d}{2\xi}\right) - \arcsin(i) + \frac{d}{2\xi}\sqrt{1-\left(\frac{d}{2\xi}\right)^2} - \\ i\left(\sqrt{1-i^2} + arcsin\left(\frac{d}{2\xi}\right) + \frac{d}{2\xi}\sqrt{1-\left(\frac{d}{2\xi}\right)^2} - \frac{\pi}{2}\right) \end{array}\right) - \alpha_e\, \xi^2 (2-\sqrt{1-i^2})\sqrt{1-i^2} \quad (3)$$

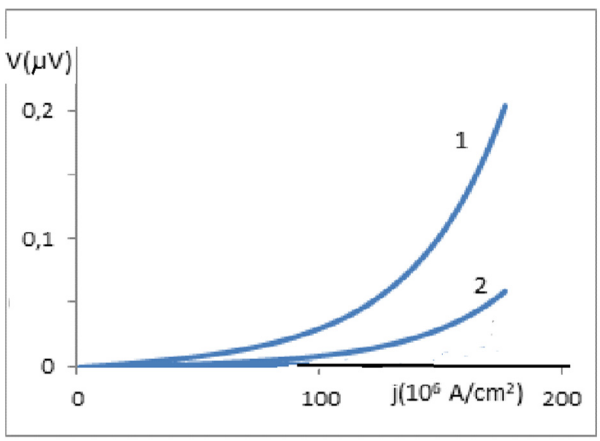

Figure 2: Influence of the elasticity parameter α_e on the current-voltage characteristics of HTc superconductor for: (1) $\alpha_e = 25 \cdot 10^{-5}$ [J/m^2], (2) $\alpha_e = 20 \cdot 10^{-5}$ [J/m^2], for B = 1 [T], T = 20 [K].

In this equation parameter $i = I/I_C$ is the electric transport current normalized to critical current I_C., while parameter α_e describes the elasticity properties of the vortex lattice. Basing on an analysis of the potential barrier the current-voltage characteristics of the HTc superconducting material have been determined for the vortex movement in the flux creep forward and backward process between nearest nano-sized defects, acting as the pinning centers, according to the relation:

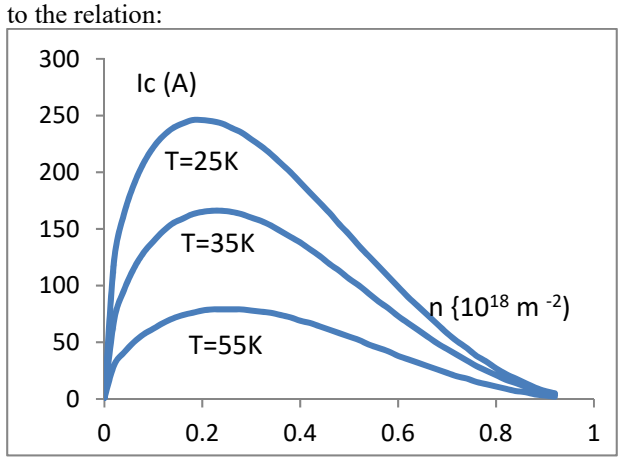

Figure 3: Calculated dependence of the critical current versus nano-defects concentration as function of temperature.

$$E = -B\omega a\left(e^{\frac{-\Delta(0)(1+i)}{k_B T}} - e^{\frac{-\Delta(i)}{k_B T}}\right) \quad (4)$$

In Eq. (4) T is temperature, k_B Boltzmann's constant, ω frequency of the flux creep process, between nearest capturing centers located at the distance of a, while potential barrier Δ(i) is described by the Eq. (3). In Fig. 2 are shown the results of the calculations current-voltage characteristics according to the above model as the function of elasticity forces of vortex lattice, expressed by parameter α_e.

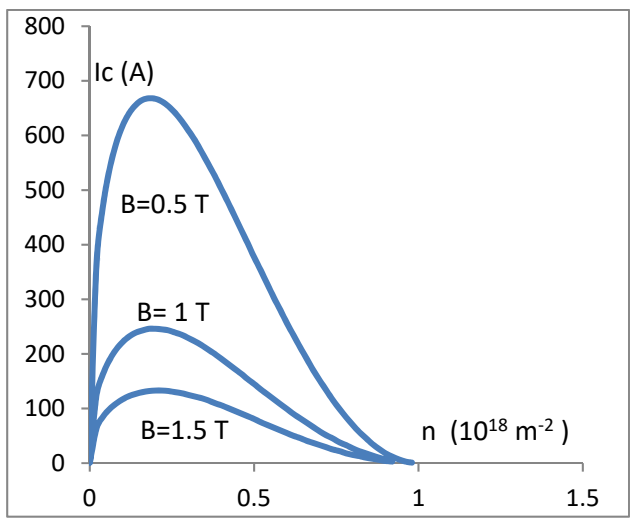

Figure 4: Calculated dependence of the critical current versus nano-defects concentration as function of magnetic induction.

It follows from Fig. 2 that with increase of the elasticity parameter critical current decreases. Critical current, determined from these characteristics filling the electric field criterion is very sensitive, especially to nano-defects concentration. In Figs. 3-5 are presented calculated dependences of the critical current determined basing on above model for half-captured initially vortices, versus the nano-sized defects concentration, which are created during the

ISBN: 978-3-95450-233-2 ISSN: 2673-5504 doi:10.18429/JACoW-SRF2021-THPFDV002

RF irradiation process. In Fig. 3 are shown results of calculations critical current as function of nano-defects concentration for various temperatures, while in Fig. 4 as function of magnetic induction. In Fig. 5 are given the results of calculations critical current versus defects concentration as function of their size. From each of these cases follows, that initially critical current increases with defects (irradiation) concentration, while then destructive effects start to dominate. Critical current finally disappears analogously as it is in the case of pure non-irradiated superconductors.

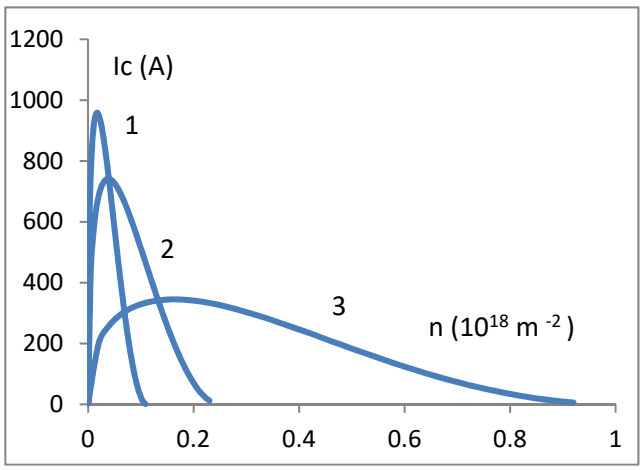

Figure 5: Calculated dependence of the critical current versus defects concentration as the function of the nano-metric defects size: (1) 3 nm, (2) 2 nm, (3) 1 nm.

IMPACT OF IC ON DYNAMIC LOSSES IN SUPERCONDUCTING CURRENT LEADS

Presented above critical current analysis of the irradiated materials has especial meaning in the case of the superconducting RF accelerators, in which appear just superconducting elements, such as electromagnets, cavities and current leads working in the irradiation environment.

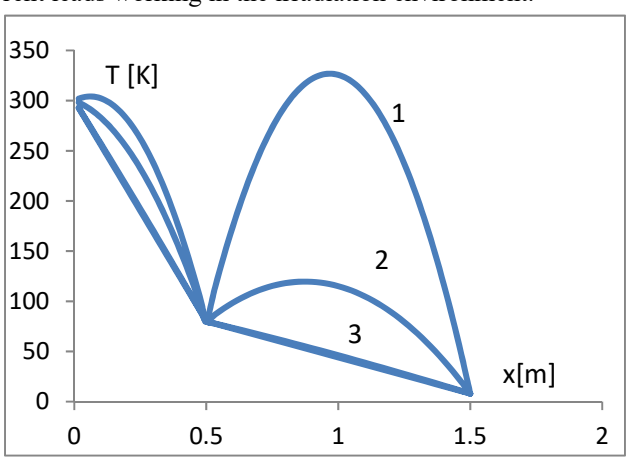

Figure 6: Calculated temperature distribution in the copper current lead with the thermal intercept at 80 K for three current amplitudes: (1) 30 A, (2) 20 A, (3) 5 A.

The main advantage of using superconductors for current leads in comparison to copper rods analysed in Fig. 6 is the lack of their resistivity, although this statement concerns stationary case only below critical current. In dynamic situation arise the electromagnetic losses generated during the current pulse flowing through the superconductors. They are a superposition of the resistive, ohmic type losses leading to the Joule heating, as well as electromagnetic losses connected with the hysteresis form of the time variation of the magnetic induction in the superconducting wire during the current cycle. These losses are described by the relation $L_e = \vec{j}\cdot\vec{E}$, in which L_e is the density of generated electromagnetic losses on the unit volume of the superconducting material, j is current density, while E electric field generated during variation of magnetic induction in the current cycle. For determination of the stationary Joule type losses in superconductors in unit volume L_J we use a power-like expression for the description of the electric field and then obtain the result: $L_J = \kappa\, j\, (j/j_c)^n$. Here κ is the material coefficient of the proportionality, n power exponent, j_c critical current density. For j smaller than j_c these losses rapidly decrease, which result indicates on the advantage of using the superconducting bars as the current leads instead of the conventional made from the normal copper, analysed in Fig. 6. A disadvantage is the cost of superconductors and necessity of cooling them, which however, for HTc materials requires only liquid nitrogen bath. Let compare losses generated in both cases. In the case of the copper lead of the length of 1 m and cross-section 1 cm^2 for the 10 kA current and copper room temperature resistivity of $\rho = 1{,}68\cdot10^{-8}\ \Omega\cdot m$, losses per unit volume reach the value of $1{,}68\cdot10^4$ W. The electric field in the 1 m long rod then brings the value of 1,68 V. For a superconducting bus however the generated electric field E in the resistive state is approximated by the power-like law mentioned before: $E = \kappa(j/j_c)^n$. Here power exponent n, for the low temperature superconductors as NbTi is equal to about 10, while for HTc superconducting leads it will be smaller. Electric field is equal in the superconducting wires at the begin of the resistive state to about 100 μV/m. For the same current of the range of 10 kA, losses in the superconducting wires are then equal to 1 W, which result indicates on the advantage of using superconductors in high power current leads, especially with high critical temperature. We remind that currently highest critical temperature of superconducting material exceeds the room temperature at hydrogen compounds but under very high pressure [4]. However, beside these Joule type losses there arise in superconducting wire, through which flows time-varying current also electromagnetic losses connected with the specific for superconductors dynamic effect of the penetration of magnetic induction in the form of vortices, also dependent on critical current discussed previously. It leads then to the generation of the electric field according to Maxwell's law: $\oint_{\partial\sigma} Edl = -\frac{\partial\phi}{\partial t}$, where $\Phi = \vec{B}\cdot\vec{S}$ is magnetic flux penetrating the closed loop of the surface S. For the electric current linearly varying in time, total losses are then the superposition of both these complementary mechanisms: resistive and dynamic losses. Fig. 7 shows the profiles of the magnetic induction distribution during the transport

ISBN: 978-3-95450-233-2 ISSN: 2673-5504 doi:10.18429/JACoW-SRF2021-THPFDV002

current cycle. Here is shown schematic picture of the penetration of magnetic induction during the increase with time of the current up to the maximal value I_m, after which current decreases to null. Direction of the induction change and the profile of the magnetic induction following it, is denoted in this figure by arrows. After decrease of the current in the cycle up to null, the remanent magnetic induction is retained in the bulk of the superconductor, which profile is described schematically by the shape of the triangle shown at the bottom of Fig. 7. Following it, increase in the current during the subsequent cycles of the applied triangular current, gives the magnetic induction profile denoted by arrow ↑ in the Fig. 7.

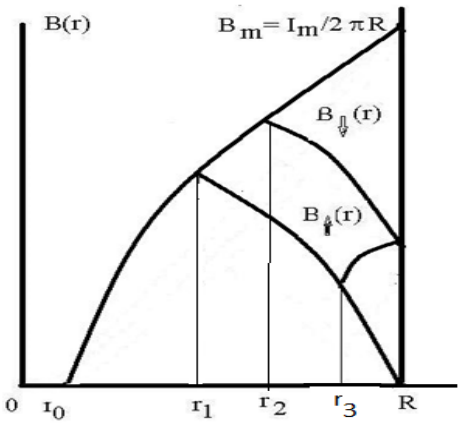

Figure 7: Magnetic induction distribution profiles in the superconductor for the first and following cycles of the electric current up to the maximal amplitude I_m, flowing through the superconducting rod of the thickness 2R. Arrows ↑ and ↓ indicate, on the current change.

For describing these dynamic losses, magnetic induction distribution in the superconducting rod through which flows the current is evaluated using the critical state approximation. According to it, at first linear in time rise of the transport electric current $I = \alpha t$, flux penetrates the sample up to the depth r_0 shown in Fig. 7:

$$r_0 = R \cdot \sqrt{1 - I/I_c} \tag{5}$$

Here I_c is the critical current of the superconducting rod determined by the relation $I_c = \pi R^2 j_c$, α – the time derivative of the current ramp, t –time, while the intensity of flowing transport current is connected with the depth r_0 by the relation:

$$I = \pi j_c (R^2 - r_0^2) = I_c - \pi j_c r_0^2 \tag{6}$$

From the above Eqs. 4 - 6 the magnetic induction profile has been calculated for the first increase of the current:

$$B_{1\uparrow}(r) = \frac{\mu_0 I_c}{2\pi r} \cdot \left(\frac{r^2}{R^2} - 1 + \frac{I}{I_c}\right) \tag{7}$$

which leads to the following form of the magnetic flux created in the unit length of the superconductor, according to the notation of Fig. 7.

$$\emptyset_{1\uparrow}(r_0, R) = \frac{\mu_0 I_c}{4\pi}\left[\left(1 - \frac{I}{I_c}\right) \cdot ln\left(1 - \frac{I}{I_c}\right) + \frac{I}{I_c}\right] \tag{8}$$

From Eq. (8), variation of this magnetic flux with time, which determines the generated electric field in a unit length of wire, is calculated:

$$\frac{\partial \emptyset_{1\uparrow}}{\partial t} = -\frac{\mu_0 \alpha}{4\pi} \ln\left(1 - \frac{I}{I_c}\right) \tag{9}$$

Basing on these equations, the losses generated during first, initial increase of electric current have been determined:

$$L_{1\uparrow} = -\frac{\mu_0 \alpha}{4\pi} \mathrm{I} \cdot \ln\left(1 - \frac{I}{I_c}\right) \tag{10}$$

For decreasing current the magnetic induction profiles marked in Fig. 7 by arrow ↓ are described by the relations:

$$\mathrm{B}_{\downarrow}(r) = \frac{\mu_0 I_c}{2\pi r} \cdot \left(\frac{I_m}{I_c} - 1 + \frac{r^2}{R^2}\right) \quad \text{for } r_0 < r < r_2 \tag{11}$$

and

$$\mathrm{B}_{\downarrow}(r) = \frac{\mu_0 I_c}{2\pi r} \cdot \left(1 + \frac{I}{I_c} - \frac{r^2}{R^2}\right) \quad \text{for } r_2 < r < R \tag{12}$$

Length r_2 shown in Fig. 7 and appearing in Eqs. (11) (12) is given then by:

$$r_2 = R\sqrt{1 - \frac{I_m - I}{2I_c}} \tag{13}$$

For the current decreasing to null in the full cycle this branch of the magnetic induction profile is described by:

$$\mathrm{B}_{0\downarrow}(r) = \frac{\mu_0 I_c}{2\pi r} \cdot \left(1 - \frac{r^2}{R^2}\right) \quad \text{for } r_1 < r < R \tag{14}$$

where

$$r_1 = R\sqrt{1 - \frac{I_m}{2I_c}} \tag{15}$$

Total current flowing inside the depths (r_0, r_2) and (r_2, R) is then respectively equal: $(I_m+I)/2$ and $(I - I_m)/2$. Following this decrease of the current, in the subsequent n-th cycle, current increases and then the magnetic induction at the depth inside the sample of the range $r_3 < r < R$, shown in Fig. 7, is mathematically given by:

$$B_{2\ldots n,\uparrow}(r) = \frac{\mu_0 I_c}{2\pi r}\left[\frac{r^2}{R^2} - 1 + \frac{I}{I_c}\right] \tag{16}$$

The current flowing then in the outer part of the wire is given by:

$$I(r) = I_c\left(\frac{r^2}{R^2} - 1 + \frac{I}{I_c}\right) \quad \text{for } r_3 < r =< R \tag{17}$$

and magnetic induction for that range of the depth inside the sample is described by:

$$B_{2\ldots n,\uparrow}(r) = \frac{\mu_0 I_c}{2\pi r}\left[\frac{r^2}{R^2} - 1 + \frac{I}{I_c}\right] \tag{18}$$

where

$$r_3 = R\sqrt{1 - \frac{I}{2I_c}} \tag{19}$$

The magnetic flux penetrating onto the depth r_3, for the unit length of superconductor, caused by the increasing current flow in the second and next increasing cycles of the current pulses is given therefore by the relation:

$$\emptyset_{2\ldots n,\uparrow}(r_3, R) = \frac{\mu_0 I_c}{4\pi}\left[\left(1 - \frac{I}{I_c}\right)\ln\left(1 - \frac{I}{2I_c}\right) + \frac{I}{2I_c}\right] \tag{20}$$

ISBN: 978-3-95450-233-2 ISSN: 2673-5504 doi:10.18429/JACoW-SRF2021-THPFDV002

The time derivative of this flux is:

$$\frac{\partial \emptyset_{2\ldots n,\uparrow}(r_3,R)}{\partial t} = -\frac{\mu_0 \propto}{4\pi}\left[\ln\left(1-\frac{I}{2I_c}\right)+\frac{I}{2(I-2I_c)}\right] \quad (21)$$

while the electromagnetic losses generated in unit length of the superconductor connected with the magnetic induction variation inside the sample on the depth r_3 - R, in the second and further ramping increase of current are therefore equal to:

$$L_{2\ldots n,\uparrow}(r_3,R) = -\frac{\mu_0 \alpha I}{8\pi}\left[\ln\left(1-\frac{I}{2I_c}\right)+\frac{I}{2\cdot(I-2I_c)}\right] \quad (22)$$

Now we shall determine losses generated in the current lead for the depth r inside the sample of the range $r_1 < r < r_3$, where magnetic induction distribution is given by:

$$B_{2\ldots n,\uparrow}(r) = \frac{\mu_0 I_c}{2\pi r}\left[1-\frac{r^2}{R^2}\right] \quad (23)$$

while current flowing in this region has the amplitude $I(r_1,r_3) = (I_m - I)/2$. Time dependent magnetic flux penetrating this region of superconducting busbar brings the value:

$$\emptyset_{2\ldots n,\uparrow}(r_1,r_3) = \frac{\mu_0 I_c}{4\pi}\left[\ln\left(2-\frac{I}{I_c}\right)-\ln\left(2-\frac{I_m}{I_c}\right)+\frac{I-I_m}{2I_c}\right] \quad (24)$$

while its time derivative is:

$$\frac{\partial \emptyset_{2\ldots n,\uparrow}(r_1,r_3)}{\partial t} = \frac{\mu_0 \propto}{8\pi}\frac{I}{(I-2I_c)} \quad (25)$$

Generated in this region losses are equal therefore:

$$L_{2\ldots n,\uparrow}(r_1,r_3) = \frac{\mu_0 \alpha I}{16\pi}\frac{(I_m-I)}{(2I_c-I)} \quad (26)$$

Finally generated total losses during the enhancement of current in the second and next current cycles are equal to:

$$L_{2\ldots n,\uparrow}(r_0,R) = \frac{\mu_0 \alpha I}{8\pi}\left[\frac{I_m}{2\cdot(2I_c-I)}-\ln\left(1-\frac{I}{2I_c}\right)\right] \quad (27)$$

The results of the calculations of electromagnetic losses connected with the change during current rise magnetic induction inside superconducting rod are shown in Fig. 8.

Figure 8 presents the results of the calculations of the electromagnetic losses created at increasing current in the first and subsequent current pulses at superconducting leads. Shown here data indicate on the hysteresis behavior of electromagnetic losses in superconductors and have technical meaning onto which proves the decrease of losses in subsequent current cycles in comparison to the first one. It additionally shows on the advantages of using superconducting materials in the energy devices as current leads in the RF accelerators, because consume much less energy especially in the following current cycles, than conventional busbars. This effect has therefore especial meaning at the construction RF superconducting apparatus.

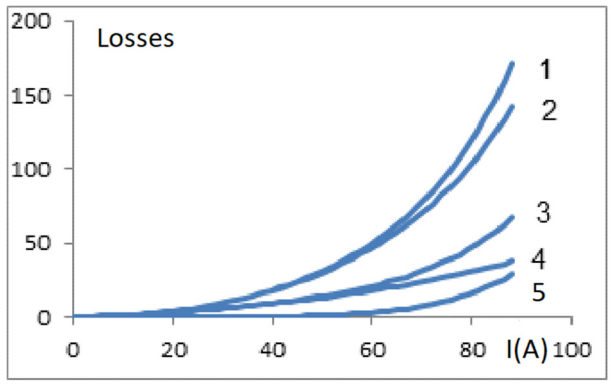

Figure 8: Dependence of the losses generated in HTc superconducting lead on the linearly varying current of the maximal amplitude $I_m = 90$ A, $I_c = 110$ A, $n = 5$ for the case of: (1) Losses generated in the first rise of the linearly varying current and ohmic losses, (2) Losses generated in the first growth of the linearly varying current, (3) Losses generated in subsequent increases of the linearly varying current and ohmic losses, (4) Losses generated in subsequent increases of the linearly varying current and (5) pure ohmic Joule type losses.

REFERENCES

[1] J. Sosnowski, "Superconducting cryocables", Book Publisher of *Electrotechnical Institute*, in Polish, pp. 1-100, 2012.

[2] J Sosnowski, "Modelling of the influence of heavy ions irradiation on the current-voltage characteristics of the HTc superconducting tapes subjected to the bending strain process", in *Proc. SPIE 11054, Superconductivity and Particle Accelerators*, 2018.

[3] J Sosnowski, "Analysis of electric current flow through the HTc multilayered superconductors", *IOP Conf. Ser.: Mater. Sci. Eng.*, vol. 113, p. 012019, 2016.

[4] A.P. Drozdov, M.I.Eremets, I.A.Troyan, V. Ksenofontov, S.I. Shylin, "Conventional superconductivity at 203 kelvin at high pressures in the sulfur hydride system" in *Nature Letter,* vol. 525, pp. 73-76, 2015.